Time-Resolved Explosion of Intense-Laser-Heated Clusters

K. Y. Kim, I. Alexeev, E. Parra, and H. M. Milchberg
Institute for Physical Science and Technology, University of Maryland, College Park, Maryland 20742
(Received 10 June 2002; published 14 January 2003)

We investigate the femtosecond explosive dynamics of intense laser-heated argon clusters by measuring the cluster complex transient polarizability. The time evolution of the polarizability is characteristic of competition in the optical response between supercritical and subcritical density regions of the expanding cluster. The results are consistent with time-resolved Rayleigh scattering measurements, and bear out the predictions of a recent laser-cluster interaction model [H. M. Milchberg, S. J. McNaught, and E. Parra, Phys. Rev. E **64**, 056402 (2001)].

DOI: 10.1103/PhysRevLett.90.023401 PACS numbers: 36.40.Vz, 36.40.Gk, 52.50.Jm

Intense laser interaction with clusters, van der Waals-bonded agglomerations of up to $\sim 10^7$ atoms, is of much current interest owing to applications which include the generation of x rays [1], fast electrons and ions [2], and nuclear particles [3], as well as control of beam propagation [4] and phase matching [5]. The manner in which a laser-driven cluster explodes in the intense field should strongly determine the details of the laser coupling, but there is still uncertainty over how this happens.

Recently, several laser-cluster interaction models have been developed [6–9]. For small clusters of a few hundred atoms or less, laser-heated electrons can easily escape the cluster early in the interaction, leaving electrostatic forces between the ions to drive cluster disassembly ("Coulomb explosion") [7]. For larger clusters composed of greater than $\sim 10^3$ atoms, hydrodynamic forces dominate [6,7,9]. The earliest and most often cited plasma hydrodynamic model assumes that a laser-heated cluster expands at uniform density [9]. This model qualitatively explains the observation of high ionization stages [1], energetic electrons and ions [2], and resonant behavior in the laser-cluster coupling [9–12]. The assumption of uniform density expansion results in the near-field cluster response $\mathbf{p} = \gamma\mathbf{E} = a^3(\frac{\varepsilon-1}{\varepsilon+2})\mathbf{E}$, where $\mathbf{p}$ is the induced dipole moment of the cluster, $\mathbf{E}$ is the laser field, γ is the cluster polarizability, a is the cluster radius (where $ka \ll 1$), and $\varepsilon = 1 - \xi + i(\nu/\omega)\xi$ is the dielectric function of the plasma internal to the cluster, taken to be of the Drude form. Here $\xi = (1 + \nu^2/\omega^2)^{-1}N_e/N_{\rm cr}$, N_e is the electron density, $N_{\rm cr} = m\omega^2/4\pi e^2$ is the critical density (m and e are the electron mass and charge), ν is the collision frequency, and $\omega = ck$ is the laser frequency. Resonant laser-cluster coupling occurs when $\varepsilon + 2 = 0$, or $N_e/N_{\rm cr} \sim 3$. As the cluster expands at the plasma sound speed c_s, the duration of the resonance is $\delta t_{\rm res} \approx \frac{2}{3}\frac{\nu}{\omega}(\frac{N_{e0}}{3N_{\rm cr}})^{1/3}\frac{a_0}{c_s}$ for initial radius a_0 and electron density N_{e0} [6]. For typical clusters having a_0 up to a few hundred Å, $\delta t_{\rm res} < 10$ fs, an interval much shorter than the apparent picosecond time scale for resonance indicated by recent absorption/scattering [10] and x-ray [11,12] measurements.

In this Letter, we measure the transient complex polarizability of argon clusters under intense pump laser illumination. We show that both this measurement and a complementary time-resolved Rayleigh scattering measurement verify the main features of our laser-cluster interaction model [6], in which the laser couples resonantly at the critical density region of the expanding clusters. This implies that clusters explode "layer-by-layer" rather than at uniform density. This determination has significant consequences for applications.

A schematic of the experimental arrangement is shown in Fig. 1. Moderate energy (1 mJ) 800 nm, 80 fs pump pulses from a 10 Hz Ti:sapphire laser system were focused onto a pulsed supersonic gas jet backed with high pressure argon gas. The peak vacuum laser intensity was $\sim 1 \times 10^{15}$ W/cm^2 in an ~ 25 μm FWHM focal spot, with a confocal parameter of ~ 3.5 mm. The gas jet was operated in the backing pressure range 150–400 psi. Cluster size estimates using the Hagena parameter [13] for our nozzle conditions [11] give average argon cluster radii in the range 150–300 Å.

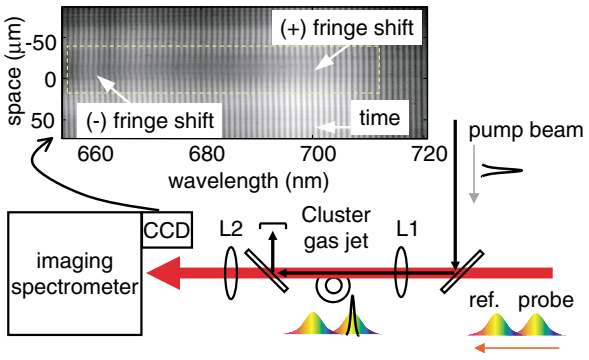

FIG. 1 (color online). Experimental setup, showing pump beam and chirped supercontinuum (SC) reference and probe pulses combined at beam splitter BS and focused by lens L1 through the edge of a cluster jet. The pump is dumped and the reference and probe SC pulses are relayed by L2 to the imaging spectrometer where they interfere, producing a spectral interferogram (example shown).

Our experiment determines the ensemble-average transient polarizability $\bar{\gamma}$ of the gas of laser-heated argon clusters, which is related to the refractive index n by $n = (1 + 4\pi N_c \bar{\gamma})^{1/2} \approx 1 + 2\pi N_c \bar{\gamma}$, where N_c is the number of clusters per unit volume. The transient index n was measured using single-shot supercontinuum spectral interferometry, a technique we have recently developed [14]. Approximately 1 mJ was split from the main Ti:sapphire pulse and was focused in 1 atm air to produce a broad, 150 nm FWHM supercontinuum (SC) extending mainly to the short wavelength side of the pump pulse. After spatial filtering, the ~0.1 mJ SC pulse was recollimated and split into equal energy probe and reference pulses. Temporal chirp of the SC to ~1.5 ps was imposed on the pulses by a 25.4 mm thick SF4 glass window. The twin chirped SC pulses were recombined with the pump and collinearly focused with it into the interaction region, with the reference pulse leading the pump, and the probe superimposed on it. The SC beam was focused to a ~170 μm FWHM spot size, overfilling the pump spot. The pump and SC beams were focused laterally away from the jet center so that the path length through the cluster gas was ~1 mm. (The central path through the jet was ~3 mm.) This eliminated the effects of probe beam refraction from the pump-induced index profile. The SC pulses were imaged from the exit of the jet onto the entrance slit of a spectrometer, providing 1D transverse space resolution. A CCD camera in the spectrometer's focal plane recorded the spectral interferogram of the reference and probe pulses, from which the time dependent phase shift $\Delta\phi(x, t)$ and absorption $A(x, t) = 1 - \exp[-\eta(x, t)]$ of the probe pulse were extracted with 15 fs resolution in a temporal window up to 1.5 ps long [14]. Here x is the transverse dimension ($x = 0$ is the pump beam axis), and η is the small signal absorption coefficient. The refractive indices $n_r = \mathrm{Re}(n)$ and $n_i = \mathrm{Im}(n)$ are related by $\Delta\phi(x, t) = k_{\mathrm{pr}}[n_r(x, t) - 1]L$ and $\eta(x, t) = k_{\mathrm{pr}} n_i(x, t)L$, where $L = 1$ mm is the interaction length through the cluster jet and $k_{\mathrm{pr}} = 2\pi/\lambda_{\mathrm{pr}}$, where $\lambda_{\mathrm{pr}} = 700$ nm is the SC central wavelength.

Figure 2(a) shows $\Delta\phi(x = 0, t)$ and $\eta(x = 0, t)$ (and $n_r - 1$ and n_i) for a range of backing pressures. The phase shifts $\Delta\phi$ are all positive for several hundred femtoseconds, and then go negative and saturate at constant negative values. With increasing backing pressure, the zero crossing moves to longer times and the relaxation to saturation occurs on increasing time scales. By contrast, laser ionization of a nonclustering helium gas jet shows purely negative-going phase shifts whose rise times are independent of jet backing pressure [15]. The peak for each η curve occurs near the zero crossing point for its corresponding $\Delta\phi$. The curves for η broaden and the peaks move to longer times with increasing backing pressure. Figure 2(b) shows a 2D grayscale plot of $\Delta\phi(x, t)$ for the 350 psi case. Note that the positive-going spatial profile for $\Delta\phi$ at early times shows that ultrafast laser-heated cluster gas can act as an optical self-guiding medium [4].

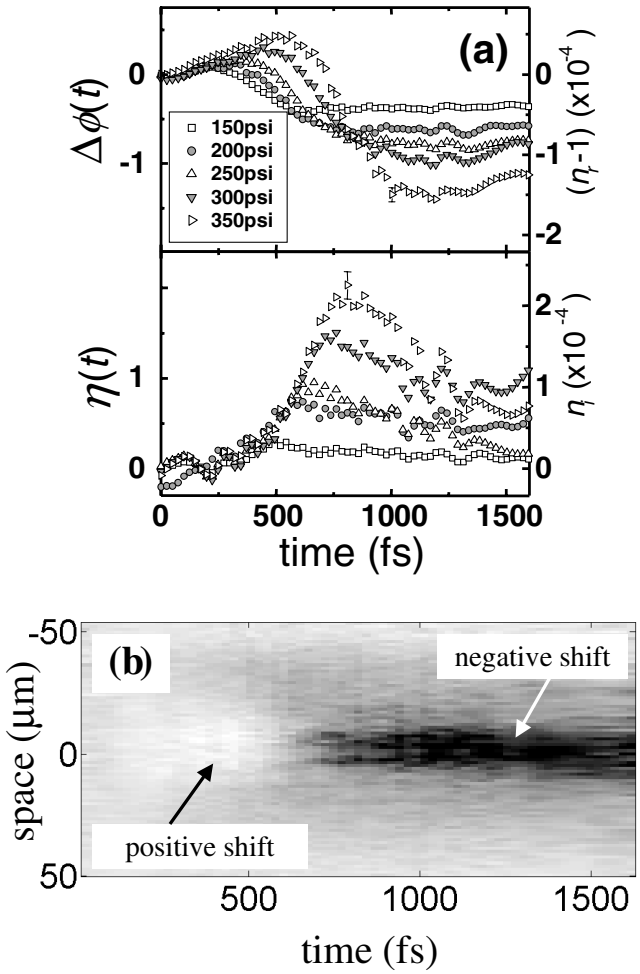

FIG. 2. (a) Top: Phase shift $\Delta\phi$ (left scale) and corresponding real index shift $n_r - 1$ (right scale) extracted from spectral interferograms, for backing pressures (cluster radii) 150 psi (150 Å), 200 psi (200 Å), 250 psi (235 Å), 300 psi (270 Å), and 350 psi (300 Å). Bottom: Small signal absorption coefficient η (left scale) and corresponding imaginary index n_i (right scale). Plots are 10 shot averages. The error bars shown on the 350 psi plots represent the variance. (b) A 2D plot of $n_r - 1$ versus transverse coordinate and time for the 350 psi case.

We performed a complementary measurement of Rayleigh scattering of a short, variably delayed, weak $\lambda_{\mathrm{pr}} = 400$ nm probe pulse, obtained from doubling an 80 fs, 800 nm pulse in a thin potassium dihydrogen phosphate crystal. The scattered 400 nm light was detected with a spectrally filtered photomultiplier tube at 90° to the pump beam direction. The power scattered by a cluster is proportional to $|\mathbf{p}_{\mathrm{pr}}|^2$, where $\mathbf{p}_{\mathrm{pr}} = \gamma \mathbf{E}_{\mathrm{pr}}$ is the probe-induced cluster dipole moment, $\mathbf{E}_{\mathrm{pr}}$ is the probe laser field, and γ is the cluster polarizability at λ_{pr}. For a spatially uniform field, the dependence of the side scattering versus pump-probe delay follows the evolution of $\overline{\gamma^2} \propto \sum_j |\gamma_j|^2$, a sum over clusters in the observation

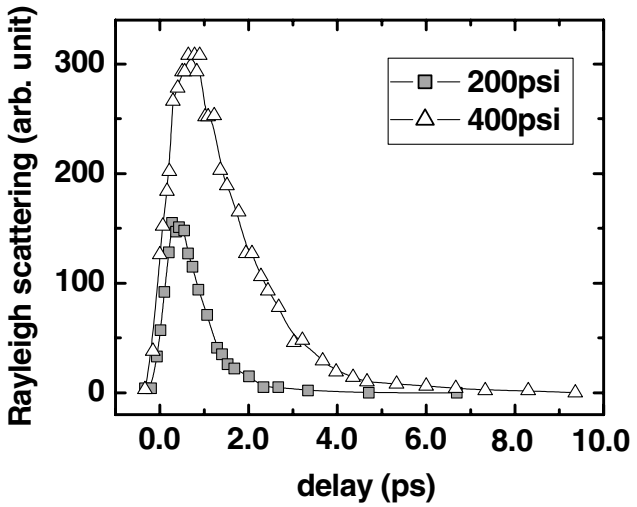

FIG. 3. The 90° Rayleigh scattered 400 nm probe signal vs pump-probe delay for backing pressures 200 and 400 psi (average cluster radii 200 and 350 Å).

volume, where cross terms in the sum have been neglected [16]. Figure 3 shows time-resolved scattering curves of increasing width for backing pressures of 200 and 400 psi (average 200 and 350 Å clusters). Although γ is smaller at 400 nm than at 700 nm for a given cluster [6], the widths of the scattering curves are in qualitative agreement with the variations of $\Delta\phi$ and η in Fig. 2(a).

The transient ensemble-average cluster polarizability $\bar{\gamma}$ is calculated by our near-field, 1D laser-cluster interaction code, the full details of which can be found in Ref. [6]. This hydrodynamic model is appropriate for clusters larger than 25 Å in radius ($\gtrsim 10^3$ atoms). The near-field treatment (for $ka_{\max} \ll 1$, where $a_{\max}$ is the expanding plasma-vacuum boundary) is satisfied for the $\sim$1.5 ps time scales of our experiment. First, the dynamics of a single cluster are calculated. Since there is little or no electronic band structure in the strongly heated cluster, the dielectric function of the cluster material is taken to be of the Drude form as described above, except that now all of its parameters are space dependent. For an incident (external) laser electric field $\mathbf{E}_L(t) = E_L(t)\hat{\mathbf{z}}$, where $\hat{\mathbf{z}}$ is the polarization unit vector, the code solves for the self-consistent scalar potential in spherical coordinates $\Phi(\mathbf{r},t) = u(r, t)\cos\theta$ inside and outside the cluster, giving the electric field $\mathbf{E}(\mathbf{r}, t) = -\nabla\Phi(\mathbf{r}, t)$. As the hydrodynamic variables are constrained to depend only on radius, we calculate the field's effect on the cluster via ionization, heating, and ponderomotive forces by using an effective field $E_{\text{eff}}(r) = \langle \mathbf{E} \cdot \mathbf{E}^* \rangle^{1/2}$, where the angle brackets represent an average over solid angle. Determination of γ is made by superimposing a very long and weak $\lambda_{\text{pr}} = 700$ nm pulse on the cluster dynamics and calculating the resulting self-consistent scalar potential $\Phi_{\text{pr}}(\mathbf{r}, t)$, which is then matched at $r > a_{\max}$ to the known analytic solution outside the cluster $\Phi_{\text{out}}(\mathbf{r}, t) = \mathbf{r} \cdot \mathbf{E}_{\text{pr}}(t) + \mathbf{r} \cdot \mathbf{p}/r^3$, where $\mathbf{p} = \gamma \mathbf{E}_{\text{pr}}$. The ensemble-average $\bar{\gamma}(t)$ is then calculated by determining $\gamma(t)$ for a range of cluster sizes and performing a weighted average over a 100% FWHM size distribution.

For a pump laser with Gaussian FWHM pulse width 80 fs, center wavelength 800 nm, and peak intensity 10^{15} W/cm^2, Figs. 4(a) and 4(b) show calculation results for $\text{Re}(\bar{\gamma}) = \bar{\gamma}_r$ and $\text{Im}(\bar{\gamma}) = \bar{\gamma}_i$ for a range of average cluster sizes with atomic density $\rho = 1.8 \times 10^{22}$ cm^{-3}. We first discuss the long time behavior of $\bar{\gamma}_r$. At times $t \gg \bar{a}_0/c_s$, the average cluster density profile will become progressively more uniform. Therefore, $\bar{\gamma}$ predicted by our model and that predicted by the uniform density model [9] should converge to $\bar{\gamma}_i \to \bar{\gamma}_{i,\text{long}} = 0$ and $\bar{\gamma}_r \to \bar{\gamma}_{r,\text{long}} = -\rho a_0^3 Z/3N_{\text{cr}} = \text{const}$, where Z is the average ionization state in the expanded plasma, which remains "frozen in" until long after cluster disassembly [6]. The values for $\bar{\gamma}_{r,\text{long}}$ are overlaid on the simulation results with dashed lines; agreement with the code results is excellent. At times greater than $\sim$1 ps, therefore, each cluster contributes an *unchanging* $\gamma_{r,\text{long}}$ to the overall

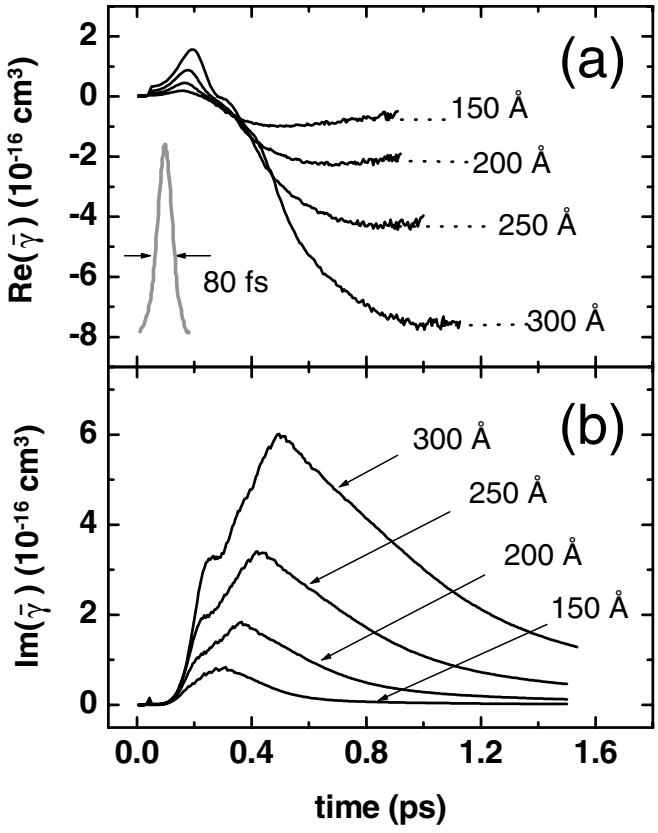

FIG. 4. (a) Calculation of $\text{Re}(\bar{\gamma}(t))$ for average cluster sizes 150–300 Å. The noise at longer times is from the numerical computation. Values for $\bar{\gamma}_{r,\text{long}}$ are shown as dotted lines. The temporal position of the pump laser pulse is shown. (b) $\text{Im}(\bar{\gamma}(t))$ for the clusters of (a). The very small peaks in $\text{Im}(\bar{\gamma})$ and steps in $\text{Re}(\bar{\gamma})$ at $t \sim 30$ fs are from the $3N_{\text{cr}}$ resonance [9], which occurs very early in the pulse before expansion takes place.

refractive index. This implies that the refractive index of a gas of exploding clusters can assume the uniform plasma value long before the clusters merge with one another. That is, $n_r = 1 + 2\pi N_c \bar{\gamma}_{r,\mathrm{long}} = 1 - N_{e,\infty}/2N_{\mathrm{cr}}$, where $N_{e,\infty}$ is the final uniform electron density of the bulk plasma. Transverse interferometry of the plasma from our 350 psi jet using a modified Mach-Zehnder interferometer [17] gives $N_{e,\infty} \sim 5 \times 10^{17}$ cm^{-3}, giving $-N_{e,\infty}/2N_{\mathrm{cr}} = -1.1 \times 10^{-4}$ for $\lambda_{\mathrm{pr}} = 700$ nm, in good agreement with the long time value of $(n_r - 1)$ for the 350 psi case in Fig. 2(a). Using the code result of $\bar{\gamma}_{r,\mathrm{long}} \sim -7.5 \times 10^{-16}$ cm^3 (for 300 Å clusters) then gives $N_c \sim 3 \times 10^{10}$ clusters/cm^3. For 300 Å clusters, this corresponds to an average $\sim 6 \times 10^{16}$ atoms/cm^3, which is consistent with our measured $N_{e,\infty}$ for $Z \sim 10$, which is itself consistent with previous extreme ultraviolet spectroscopy of argon clusters [11,12]. We note that values of $\bar{\gamma}$ predicted by our model, and verified here, are $\sim$100 times smaller than in the uniform density model [6,9]. This has a major effect on propagation [4] and on cluster heating, where the laser power coupled to a cluster is proportional to $\mathrm{Im}(\gamma)|\mathbf{E}_L|^2$ [6].

The crossover of γ_r from positive to negative values is explained as follows. The cluster dipole moment can be viewed as the integral of a dipole density over the cluster volume. That is, $\mathrm{Re}(\mathbf{p}) = \gamma_r \mathbf{E}_{\mathrm{pr}} = -\frac{1}{4\pi}\int_V d^3 r \xi \mathbf{E}_{\mathrm{int}}$, where $\mathbf{E}_{\mathrm{int}}$ is the self-consistent field internal to the cluster, and $-\xi \mathbf{E}_{\mathrm{int}}/4\pi$ is the dipole moment density. The real polarizability $\gamma_r > 0$ when the integral is dominated by regions where $N_e > N_{\mathrm{cr}}$, so the material is locally polarized so as to oppose the external field. Under these conditions, the cluster responds to the external field like an oscillator driven below its resonant frequency. In the opposite limit of $\gamma_r < 0$, the subcritical $N_e < N_{\mathrm{cr}}$ response dominates the integral. The response eventually relaxes to that of a sum of individual electrons, or a subcritical bulk plasma ($\gamma_r \rightarrow \gamma_{r,\mathrm{long}}$). For larger clusters, the crossover occurs at longer times because there are more cluster "layers" to blow off toward subcritical density. The increase of γ_i over a few hundred femtoseconds corresponds to the evolution of the critical density layer on the cluster, and its decrease to zero at longer times occurs as the cluster average density drops below critical and continues lower.

The calculation reproduces the main features of the experimental results shown in Fig. 2. For larger clusters, the zero crossing of $\bar{\gamma}_r$ $(n_r - 1)$ takes place at longer times and relaxation to the bulk response is slower. The peaks of $\bar{\gamma}_i$ (n_i) take place at longer times and the widths increase. The main difference between the experiment and calculation is that the calculation underestimates (by $\sim 2\times$) the ratio of peak positive to negative excursion of $\bar{\gamma}_r$. This may be related to an overestimation of the early time shielding of the laser field by the cluster plasma or to limitations of the 1D model. A full 3D model, however, would still show resonant coupling at the critical density region and the intracluster competition between the above critical and below critical density responses. It is that competition which is revealed by the experiment and which tells us how the cluster explodes.

This work is supported by the National Science Foundation and the U.S. Department of Energy.

[1] A. McPherson *et al.*, Phys. Rev. Lett. **72**, 1810 (1994).
[2] Y. L. Shao *et al.*, Phys. Rev. Lett. **77**, 3343 (1996); V. Kumarappan *et al.*, Phys. Rev. Lett. **87**, 085005 (2001).
[3] T. Ditmire *et al.*, Nature (London) **398**, 489 (1999).
[4] A. Gupta, T. M. Antonsen, and H. M. Milchberg, Bull. Am. Phys. Soc. **46**, 201 (2001) (http://www.aps.org/meet/DPP01/baps/abs/S1400099.html); I. Alexeev, K. Y. Kim, T. Antonsen, and H. M. Milchberg (to be published).
[5] J. W. G. Tisch, Phys. Rev. A **62**, R041802 (2000); T. Tajima *et al.*, Phys. Plasmas **6**, 3759 (1999).
[6] H. M. Milchberg, S. J. McNaught, and E. Parra, Phys. Rev. E **64**, 056402 (2001).
[7] M. Lezius *et al.*, Phys. Rev. Lett. **80**, 261 (1998).
[8] W. A. Schroeder *et al.*, J. Phys. B **31**, 5031 (1998); C. Rose-Petruck *et al.*, Phys. Rev. A **55**, 1182 (1997).
[9] T. Ditmire *et al.*, Phys. Rev. A **53**, 3379 (1996); T. Ditmire *et al.*, Phys. Rev. A **57**, 369 (1998).
[10] J. Zweiback, T. Ditmire, and M. D. Perry, Phys. Rev. A **59**, R3166 (1999); Opt. Express **6**, 236 (2000).
[11] E. Parra *et al.*, Phys. Rev. E **62**, R5931 (2000).
[12] I. Yu. Skobelev *et al.*, Zh. Eksp. Teor. Fiz. **121**, 1124 (2002) [Sov. Phys. JETP **94**, 966 (2002)].
[13] O. F. Hagena and W. Obert, J. Chem. Phys. **56**, 1793 (1972); O. Hagena, Rev. Sci. Instrum. **63**, 2374 (1992).
[14] K. Y. Kim, I. Alexeev, and H. M. Milchberg, Appl. Phys. Lett. **81**, 4124 (2002).
[15] K. Y. Kim, I. Alexeev, and H. M. Milchberg, Opt. Express **10**, 1563 (2002).
[16] An interesting complication is that Rayleigh side scattering can be partially coherent because $N_c \lambda_{\mathrm{pr}}^3 < 1$.
[17] I. Alexeev, K. Y. Kim, and H. M. Milchberg, Phys. Rev. Lett. **88**, 073901 (2002).